

# S3E: A Mult-Robot Multimodal Dataset for Collaborative SLAM

Dapeng Feng, Yuhua Qi, Shipeng Zhong, Zhiqiang Chen,  
Qiming Chen, Hongbo Chen, Jin Wu *Member, IEEE*, and Jun Ma

**Abstract**—The burgeoning demand for collaborative robotic systems to execute complex tasks collectively has intensified the research community’s focus on advancing simultaneous localization and mapping (SLAM) in a cooperative context. Despite this interest, the scalability and diversity of existing datasets for collaborative trajectories remain limited, especially in scenarios with constrained perspectives where the generalization capabilities of Collaborative SLAM (C-SLAM) are critical for the feasibility of multi-agent missions. Addressing this gap, we introduce S3E, an expansive multimodal dataset. Captured by a fleet of unmanned ground vehicles traversing four distinct collaborative trajectory paradigms, S3E encompasses 13 outdoor and 5 indoor sequences. These sequences feature meticulously synchronized and spatially calibrated data streams, including 360-degree LiDAR point cloud, high-resolution stereo imagery, high-frequency inertial measurement units (IMU), and Ultra-wideband (UWB) relative observations. Our dataset not only surpasses previous efforts in scale, scene diversity, and data intricacy but also provides a thorough analysis and benchmarks for both collaborative and individual SLAM methodologies. For access to the dataset and the latest information, please visit our repository at <https://pengyu-team.github.io/S3E>.

**Note to Practitioners**—The S3E dataset is a valuable asset for professionals in robotics and autonomous systems, offering a rich, multimodal set of data to refine Collaborative Simultaneous Localization and Mapping (C-SLAM) technologies. With synchronized streams from LiDAR, cameras, IMUs, and UWB across indoor and outdoor environments, it presents a diverse range of real-world challenges for testing and developing C-SLAM algorithms. This dataset is particularly beneficial for evaluating how robots perform in collaborative tasks, with its unique trajectory paradigms simulating various operational scenarios. Practitioners can use S3E to enhance their systems’ ability to handle dynamic environments, spatial constraints, and limited sensor overlap. However, working with S3E requires significant computational resources and expertise in C-SLAM. The complexity of the data may be daunting for those new to the field. Despite this, the S3E dataset is an excellent platform for pushing the boundaries of collaborative robotics, providing a rigorous benchmark for current technologies and a foundation for future developments.

**Index Terms**—Collaborative Simultaneous Localization and Mapping, Multi-Agent Systems, Dataset, Trajectory Paradigms

Corresponding author: Yuhua Qi (e-mail: qiyh8@mail.sysu.edu.cn)

Dapeng Feng, Yuhua Qi, Shipeng Zhong, Zhiqiang Chen, and Hongbo Chen are with Sun Yat-sen University, Guangzhou, China.

Qiming Chen is with South China Agricultural University, Guangzhou, China.

Jin Wu is with The Hong Kong University of Science and Technology, Hong Kong SAR, China.

Jun Ma is with The Hong Kong University of Science and Technology (Guangzhou), Guangzhou, China.

## I. INTRODUCTION

**C**OLLABORATIVE Simultaneous Localization and Mapping (C-SLAM) is pivotal for enabling multi-agent co-operation, thereby enhancing the robustness and efficiency of concurrent localization and mapping endeavors within a shared operational space [1]–[7]. Despite considerable progress in C-SLAM research during the past decade, issues of repeatability and benchmarking remain significant hurdles within the domain. The field is primarily constrained by two limitations. First, the complexity of C-SLAM systems, which integrate intricate software architectures and a variety of sensors, complicates the process of achieving perfect replication, thereby emphasizing the need for publicly available datasets to facilitate methodological evaluation. Second, a common method for evaluating C-SLAM solutions involves partitioning a single-agent SLAM dataset into several segments, each assigned to a distinct virtual agent [8]. However, this methodology is impractical for real-world multi-agent scenarios, given the uniform perspectives and lighting conditions that all virtual agents would encounter at intersection points.

Furthermore, the trajectory design for multi-robot scenarios must adhere to two fundamental principles. The first principle is temporal and spatial diversity. The trajectories should be designed to accommodate the varying intra- and inter-loop closures at different times and locations, thus offering complementary vantage points for the participating robots. The second principle pertains to the communication constraints. In practical applications, collaborative robots are limited to sharing information within a certain proximity. Hence, maintaining a reasonable interaction distance between robots within these regions is essential. In this paper, we introduce four trajectory prototypes that conform to diverse intra- and inter-robot closure strategies, aiming to evaluate the generalizability of C-SLAM methodologies.

Within the SLAM research community, publicly available datasets are indispensable for accelerating the development of SLAM algorithms suitable for real-world deployment. This significance stems from two primary factors. First, the execution of specialized SLAM experiments requires substantial investment in sophisticated hardware and complex software, including calibration routines and ground truth generation systems; hence, the availability of datasets substantially aids in the algorithmic development process. Second, these datasets provide a fair and impartial benchmarking framework for comparative analysis and performance assessment. Over the past decade, an array of SLAM datasets has emerged, each

contributing uniquely to the diversity of sensor modalities and the breadth of scenarios and motion types they encompass [9], [10]. Nonetheless, the preponderance of these datasets is skewed towards single-agent systems, equipped with an assortment of sensors such as cameras, inertial measurement units (IMUs), and LiDAR, which may limit their applicability to multi-agent contexts.

The limited availability of datasets specifically tailored for C-SLAM is largely due to the escalating challenges in data acquisition as the number of collaborating agents increases. Existing C-SLAM datasets, such as those from [11]–[16], predominantly feature a single cooperative paradigm with substantial spatial overlap among the robots, often overlooking cooperative strategies in areas with minimal overlap. To address this gap and bolster ongoing research in C-SLAM, we introduce S3E, a comprehensive multimodal dataset. S3E captures a variety of cooperative trajectory patterns across both outdoor and indoor settings.

Utilizing our S3E dataset as a foundation, we have conducted an extensive series of experiments employing state-of-the-art SLAM methodologies. These experiments spanned the spectrum of SLAM applications, from single-robot to collaborative scenarios, incorporating a rich array of sensor data. Our results indicate that current collaborative SLAM techniques often encounter suboptimal performance, particularly in handling inter-loop closures across certain sequences. This finding highlights the critical need for ongoing research aimed at improving the robustness and reliability of C-SLAM systems.

In conclusion, our work makes several key contributions to the field:

- We have assembled a pioneering C-SLAM dataset through the deployment of three state-of-the-art ground robots. Each robot is equipped with an advanced 16-beam 3D laser scanner, two high-resolution color cameras, a 9-axis IMU, a UWB receiver, and a dual-antenna RTK receiver. Notably, this is the first C-SLAM dataset to include UWB relative distance measurements, offering a novel dimension for research.
- To evaluate the adaptability of C-SLAM in environments with sparse overlap, we have captured extensive long-term sequences. These were obtained using four carefully crafted trajectory paradigms that account for a variety of intra- and inter-robot loop closure scenarios.
- We have undertaken an in-depth evaluation of contemporary C-SLAM techniques and their single-agent counterparts. This assessment leverages a wide array of sensor data, with a meticulous focus on the unique characteristics and performance attributes of each method.

## II. RELATED WORK

**Collaborative SLAM.** The integration of collaborative agents within the framework of SLAM presents a significant advancement, offering the potential for increased operational velocity and efficiency. This collaborative approach has the capacity to outstrip the performance of single-agent systems [17], [18]. Figure 1 demonstrates the operational concept of

Figure 1: **Animations of Dormitory\_1.** Data is captured simultaneously by a trio of Unmanned Ground Vehicles (UGVs). Each UGV initiates its journey from distinct starting points and independently explores separate areas. Upon successful detection of inter-loop closures, they exchange valuable information and collaboratively construct a globally consistent map. For optimal viewing of the animations, it is recommended to utilize *Adobe Reader* or *KDE Okular*.

C-SLAM, where a collective of robots is enabled to explore various sectors of an environment in parallel, thereby enhancing the overall efficiency of the exploration process compared to traditional single-agent methodologies.

C-SLAM systems can be differentiated based on their underlying network topologies, which include centralized, distributed, and adaptive models. In a centralized topology, a central server is tasked with the aggregation of all incoming sensory data, ensuring a unified estimation of multiple trajectories, and subsequently distributing these findings to the constituent agents [2], [19], [20]. Conversely, in distributed topologies, computational responsibilities are decentralized among the team of agents, with some systems utilizing a message broadcasting protocol for the propagation of information [21]. However, scalability becomes a formidable challenge in such distributed frameworks, particularly in scenarios involving a large number of robots, due to limitations in bandwidth and communication range.

To mitigate these challenges, adaptive strategies have been proposed, advocating for the transmission of information within the immediate communication sphere of the agents [3], [22], [23]. Swarm-SLAM [24] represents an innovative paradigm within this domain, adept at minimizing the communication load between robots while simultaneously accelerating the convergence of the SLAM process through the implementation of sophisticated prioritization algorithms for inter-robot loop closures. Moreover, hybrid approaches present a viable alternative, wherein a subset of robots engages in data processing, while others are dedicated to the application of the outcomes derived from this processing [25].

**SLAM Datasets.** High-quality and extensive datasets are indispensable for propelling advancements in SLAM research. Over recent years, there has been a commendable effort to release datasets to the research community. The KITTI dataset [9] is particularly noteworthy for its extensive and high-quality urban data, serving as a benchmark for both vision-based and LiDAR-related SLAM techniques. However, KITTI is not without limitations; it lacks perfectly synchronized

Table I: Comparative Analysis of Prominent SLAM Datasets. The abbreviations used within the table are as follows: "Sw" denotes Software Synchronization, indicating that synchronization across sensors or systems is achieved through software mechanisms; "Hw" represents Hardware Synchronization, where synchronization is managed by hardware means.

Dataset	Platform	Sensors				Time Sync.		Trajectory		Environment		Ground Truth
		Camera	IMU	LiDAR	UWB	Intra-	Inter-	Overlap	Paradigm	Indoor	Outdoor	
KITTI [9]	Car	✓	✓	✓	✗	Sw	✗	-	-	✓	✓	GNSS/INS
EuRoC [10]	UAV	✓	✓	✗	✗	Hw	✗	-	-	✓	✗	Motion Capture
UTIAS [11]	5 UGVs	✓	✗	✗	✗	Sw	NTP	Large	1	✓	✗	Motion Capture
AirMuseum [13]	3 UGVs, 1 UAV	✓	✓	✗	✗	Sw	NTP	Large	1	✓	✗	SfM
FordAV [12]	3 Cars	✓	✓	✓	✗	-	GNSS	Large	1	✗	✓	GNSS/INS
GRACO [15]	1UGV, 1UAV	✓	✓	✓	✗	Hw	-	Restricted	1	✗	✓	GNSS/INS
Kimera-Multi [14]	8 UGVs	✓	✓	✓	✗	-	-	Restricted	1	✗	✓	GPS and total-station assisted LiDAR SLAM
SubT-MRS [16]	UGVs, UAVs, Handheld	✓	✓	✓	✗	Hw	-	Restricted	1	✓	✓	3D Scanner
<b>Ours</b>	3 UGVs	✓	✓	✓	✓	Hw	GNSS, PTPv2	Restricted	4	✓	✓	RTK, GNSS/INS Motion Capture

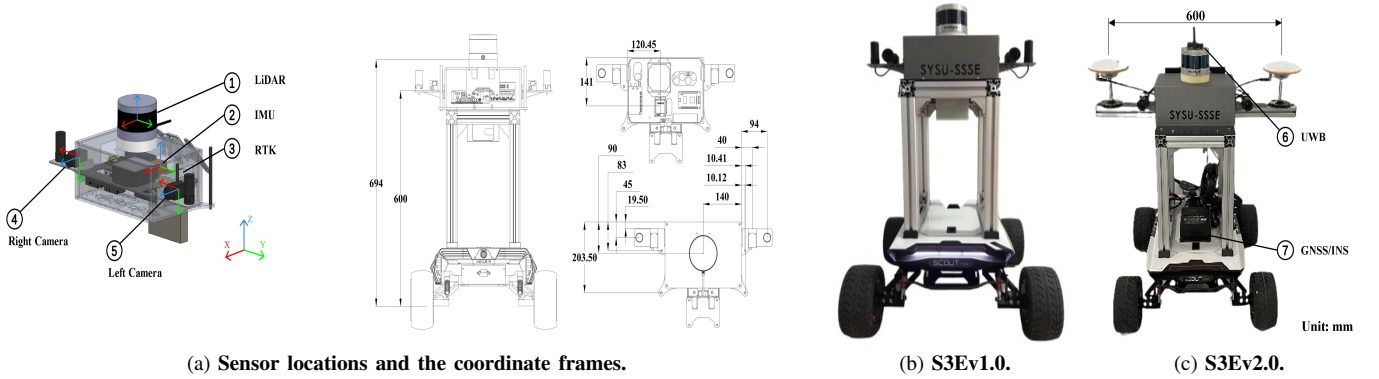


Figure 2: **Mobile Platform Sensor Layout and Coordinate Systems.** The left part details the sensor locations and the coordinate frames that define their spatial orientation relative to the platform. In the right part, our mobile platforms are available in two versions, each designed for different operational requirements.

data, offering only estimated time delays between different sensors. To surmount this limitation, the EuRoC dataset [10] was collected, providing synchronized visual and inertial data captured by a micro aerial vehicle in controlled environments, synchronized through the use of hardware clocks.

Despite these commendable efforts, there is a recognized scarcity of datasets tailored for multi-agent scenarios. The UTIAS dataset [11] stands as a pioneering work in multi-agent SLAM, featuring a collaborative system of five robots exploring a small area with identifiable landmarks. The AirMuseum dataset [13] introduces a heterogeneous multi-robot SLAM dataset within a larger warehouse environment, offering ground-truth trajectories computed using Structure-from-Motion (SfM) [26] and constrained with fixed beacons. The FordAV dataset [12] presents a dataset of multiple autonomous vehicles with a 3D map, capturing seasonal variations in dynamic urban environments. However, these datasets tend to have substantial overlap in the co-view region, which may limit the comprehensive evaluation of C-SLAM robustness.

In an effort to address the limitations of existing datasets, the GRACO dataset [15] presents a novel approach by introducing a ground-aerial dataset. This dataset leverages the drone's altitude to dynamically adjust the extent of view overlap, offering a unique perspective on multi-agent SLAM scenarios. However, GRACO exhibits some inconsistencies in the synchronization of data acquisition between aerial and ground perspectives, and it does not fully accommodate the

complexities of dynamic environments.

The SubT-MRS dataset [16] contributes to the field by providing a diverse array of multi-robot SLAM data captured across a variety of environments. This dataset enhances the representation of real-world applications and the challenges posed by different settings.

Kimera-Multi [14] further advances the state of C-SLAM datasets by offering a comprehensive collection characterized by its diverse trajectory designs and the involvement of multiple robots. This dataset is instrumental in studying the collaborative aspects of multi-agent systems.

It is crucial to acknowledge, however, that existing datasets, including GRACO, SubT-MRS, and Kimera-Multi, often do not fully consider the intricacies of collaborative trajectory patterns. The robustness of C-SLAM systems is influenced by the ability to handle intra- and inter-loop closures, a factor that is not consistently addressed in current datasets. The consideration of these collaborative patterns is essential for developing C-SLAM algorithms that can effectively operate in environments with varying levels of agent interaction and dynamic scene elements.

In this paper, we introduce a large-scale C-SLAM dataset that includes visual ambiguities and dynamic objects, captured under four distinct trajectory paradigms to assess C-SLAM generalizability under restricted overlap conditions. Our dataset also incorporates UWB relative measurement positioning, adding a significant dimension for C-SLAM research.

Table II: Payload Sensor and Ground Truth Device Specifications. It includes information about the types of sensors, their respective capabilities, and the ground truth devices used for validation and accuracy assessment.

Device	Type	Unit
LiDAR	Velodyne	
Model	VLP-16 Puck	
Channels	16	
Range	100	<i>m</i>
Accuracy	$\pm 3$	<i>cm</i>
Vertical FOV	$\pm 15$	$^\circ$
Vertical Resolution	2	$^\circ$
Horizontal FOV	360	$^\circ$
Horizontal Resolution	0.1 ~ 0.4	$^\circ$
Max. Frequency	10	<i>Hz</i>
Camera - Stereo	HikRobot	
Model	MV-CS050-10GC	
Data Interface	GigE	
Sensor Model	Sony IMX264	
Resolution	1224 $\times$ 1024	<i>pixel</i>
Dynamic Range	72	<i>dB</i>
Baseline	360	<i>mm</i>
Max. Frequency	24.2	<i>Hz</i>
Lens Model	MVL-MF0828M-8MP	
Focal Length	8	<i>mm</i>
Vertical FOV	54.97	$^\circ$
Horizontal FOV	68.46	$^\circ$
IMU	Xsens	
Model	MTi-30-2A8G4	
Gyro In-Run Bias Stability	18	$^\circ/h$
Accel In-Run Bias Stability	15	$\mu g$
Mag RMS Noise	0.5	<i>mGauss</i>
Max. Frequency	400	<i>Hz</i>
UWB	NoopLoop	
Model	LinkTrack P-B	
Max. Distance	500	<i>m</i>
Accuracy	$\pm 10$	<i>cm</i>
Max. Frequency	200	<i>Hz</i>
RTK	Femtomes	
Model	Nano-D	
RTK Accuracy	$\pm 1$	<i>cm</i>
Max. Frequency	20	<i>Hz</i>
GNSS/INS	CHCNAV	
Model	CGI-610	
RTK Accuracy	$\pm 1$	<i>cm</i>
Gyro In-Run Bias Stability	2.5	$^\circ/h$
Accel In-Run Bias Stability	15	$\mu g$
Max. RTK Frequency	20	<i>Hz</i>
Max. INS Frequency	100	<i>Hz</i>
Motion Capture	Vicon	
Model	Tracker 3.8	
Camera Model	Vero 2.2	
Num. of Cameras	17	
Position Accuracy	$\pm 1$	<i>mm</i>

For a comprehensive comparison of different datasets, including our contribution, refer to Table I.

### III. S3E DATASET

The S3E dataset has been meticulously assembled, prioritizing high temporal precision in the synchronization of data from an array of sensors. Each sensor is calibrated to a shared timescale, ensuring that the captured multi-sensory information is harmonized. This precise synchronization is facilitated by an advanced time synchronization mechanism, essential for the accurate integration and co-registration of

data across diverse modalities. For a visual representation of the sensor placement on our mobile robot platform, refer to Figure 2. Our mobile platforms are offered in two specialized versions, each tailored to meet specific operational needs:

- S3Ev1.0 (Figure 2b): Customized for indoor operations, this version boasts a compact design that guarantees exceptional maneuverability, enabling it to traverse tight indoor spaces effortlessly.
- S3Ev2.0 (Figure 2c): This enhanced version features an expanded width, accommodating a state-of-the-art, higher-precision ground truth system. The integration of an UWB module significantly bolsters the platform's localization accuracy, particularly in environments where traditional SLAM systems may falter.

The subsequent sections delve into a comprehensive description of the S3E dataset's components and their distinctive features, highlighting the meticulous approach taken to ensure the dataset's utility and reliability in advancing SLAM research.

#### A. Sensor Configuration

Our S3E dataset encompasses a multimodal array of sensors, each selected for its operational range and noise characteristics, and meticulously synchronized to capture data with high temporal precision. The sensors are integrated onto the *Agilex Scout Mini*, a versatile all-terrain mobile platform capable of high-speed remote-controlled navigation, featuring four-wheel drive and a maximum speed of 10km/h.

For a comprehensive understanding of the data acquisition process and to facilitate replicability of our experiments, Table II outlines the technical specifications of the sensors and ground truth devices that were integrated into our payload. This includes the sensor types, their resolution, measurement range, accuracy, and any other pertinent technical details that define their contribution to the SLAM system's performance.

#### B. Sensor Synchronization

This section delves into the critical processes of time synchronization and sensor calibration, which are essential for achieving optimal sensor fusion and maximizing system performance within a dynamic, multimodal environment.

1) *Time Synchronization.*: Time synchronization across all sensors is essential for the accurate co-registration of multi-sensor data, particularly in dynamic environments where precise timing is critical to the quality of the fused dataset. This synchronization ensures that data from various sensors is temporally aligned, facilitating coherent integration and analysis.

Our synchronization system is built around an *Altera EP4CE10* FPGA board acting as the primary trigger device, with an *Intel NUC11TNKv7* serving as the host computer. The system is designed with a comprehensive set of I/O interfaces to accommodate the diverse requirements of different sensors, as depicted in Figure 3.

For synchronization across agents, we address two distinct scenarios:

- In outdoor settings with access to Global Navigation Satellite System (GNSS) signals, we use GNSS time as



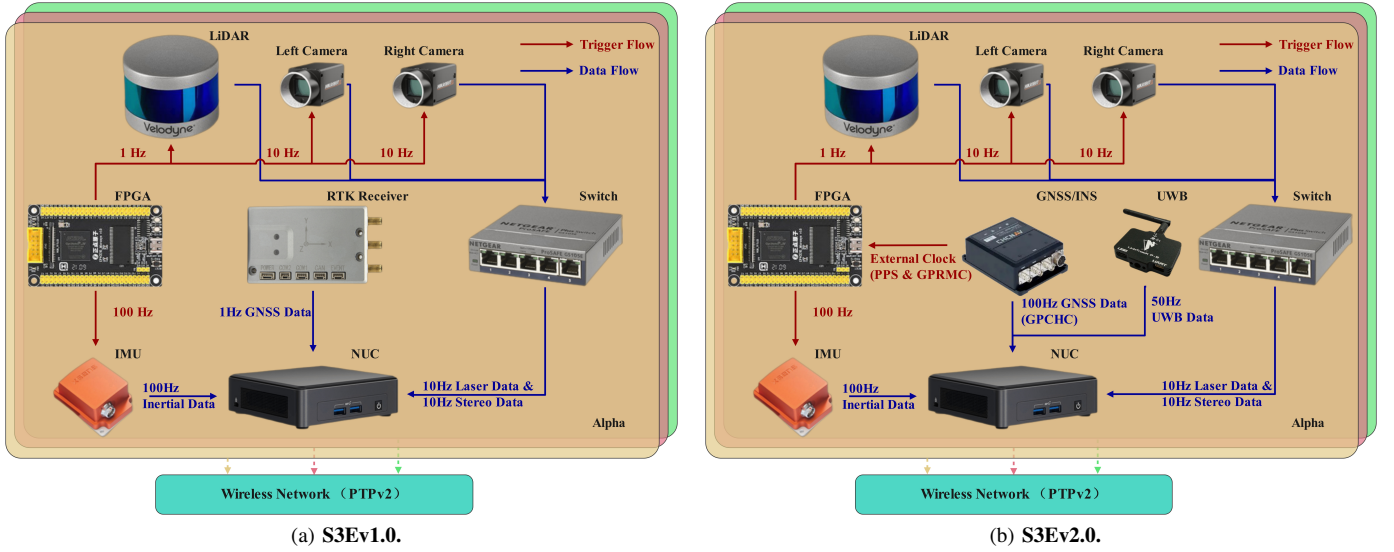


Figure 3: **Time Synchronization Scheme.** The scheme addresses synchronization in both outdoor environments using GNSS time as the global reference and in GNSS-denied environments like indoors and tunnels, where agents rely on a PTPv2 server for time synchronization.

the global reference to synchronize the timing across agents.

- In GNSS-denied environments such as indoors and tunnels, agents synchronize their timers by obtaining external global time data from Alpha, which serves as a Precision Time Protocol version 2 (PTPv2) server, via a wireless network connection.

Within each agent, the FPGA orchestrates the timing for various sensors:

- **S3Ev1.0:** The FPGA periodically issues a pulse from a low-drift oscillator to trigger the LiDAR, stereo cameras, and IMU, as shown in Figure 3a. Specifically, the FPGA generates a 1 Hz pulse to initiate the LiDAR, which then outputs data at 10 Hz and updates its internal counter register upon receiving the trigger signal. The stereo cameras and IMU are designed to immediately return data following the receipt of an FPGA trigger pulse. The FPGA is configured to generate trigger pulses at 10 Hz for the cameras and 100 Hz for the IMU, tailored to the specific data output needs of these sensors.
- **S3Ev2.0:** This version enhances synchronization by aligning the FPGA board with the pulse-per-second (PPS) signal from its internal GNSS/INS module, as depicted in Figure 3b. This alignment generates frequency trigger signals for IMU, stereo cameras, and LiDAR clock synchronization. The UWB receiver, not supporting trigger-based data acquisition, collects and outputs measured distance data directly.

Considering transmission delays, all sensor readings are forwarded to the host computer, where they are timestamped upon arrival, organized, and packaged to ensure accurate temporal referencing for subsequent analysis.

2) *Sensor Calibration.*: Our sensor suite is governed by a unified coordinate system framework, adhering to the right-hand rule, which ensures uniformity in data orientation and facilitates standardized analysis.

The calibration process was meticulously carried out in a series of five distinct stages, each designed to ensure the precise alignment and integration of sensor data:

**Camera Intrinsic Calibration:** We executed a high-precision intrinsic calibration for our cameras using the conventional checkerboard pattern, a method renowned for its reliability [27]. This process determined the camera intrinsic matrix  $K$  and the lens distortion coefficients  $D$ , which are essential for correcting lens distortions and enhancing image accuracy.

**IMU Intrinsic Calibration:** Intrinsic calibration of the IMU involved accounting for white noise  $\sigma_n$  and random walk noise  $\sigma_m$  in the measurements. Building upon the nominal values provided in the *Xsens MTi-30-2A8G4* IMU's data sheet, we refined these parameters through a calibration process utilizing Allan variance, thereby achieving a more accurate probabilistic model of IMU noise [28].

**Camera-Camera Extrinsic Calibration:** The extrinsic calibration of the stereo cameras was performed to determine the rotation matrix  $R$  and the translation vector  $t$ , which were computed by minimizing reprojection errors. This step is crucial for establishing the geometric relationship between the two cameras in a stereo setup [27].

**Camera-IMU Extrinsic Calibration:** The spatial transformation  $T_{ic}$  between the camera and IMU was ascertained using the open-source Kalibr toolbox [29]. This calibration is essential for the integration of IMU data with visual data for enhanced pose estimation and sensor fusion.

**Camera-LiDAR Extrinsic Calibration:** The extrinsic calibration between the camera and LiDAR, represented as  $T_{lc}$ , was established by minimizing line-to-plane errors, ensuring the accurate co-registration of LiDAR point clouds with camera imagery [30].

Upon completion of these calibration stages, the resulting parameters were meticulously stored in YAML files for each agent, ensuring that the calibrated parameters are readily accessible and reproducible.

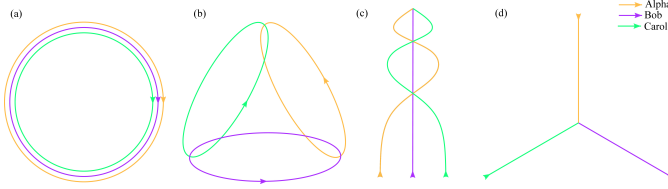


Figure 4: **Illustration of Trajectory Paradigms for C-SLAM.** The distinct trajectory paradigms adopted by three agents, designated as Alpha, Bob, and Carol, to demonstrate different interaction and information exchange patterns in a multi-agent SLAM context. (a) **Concentric Circles.** (b) **Intersecting Circles.** (c) **Intersection Curve.** (d) **Rays**

### C. Ground Truth

To establish accurate ground truth tracks for our dataset, we implement a multifaceted approach leveraging three distinct methods.

In outdoor settings where GNSS signals are readily accessible, we employ a dual-antenna Real-Time Kinematic (RTK) device to capture localization data with an accuracy reaching centimeter-level precision. For the S3Ev2.0 platform, we have made a significant advancement in our ground truth instrumentation by integrating a GNSS/INS unit. This upgrade enables high-frequency positioning data output, even during GNSS signal outages, such as those encountered in tunnel environments. The system achieves this by fusing RTK measurements with data from the built-in IMU through a post-processing fusion technique, thereby ensuring continuous and reliable ground truth data for our dataset.

In GNSS-denied environments, such as indoor laboratories, we employ a motion capture system equipped with 17 high-frequency cameras to record the start and endpoints of the tracks. This setup is utilized due to the prohibitive costs associated with constructing a large-scale motion capture system. For indoor scenarios not equipped with a motion capture system, such as in teaching buildings, we record the initial and terminal points of the tracks using the RTK device.

By combining these methods, we are able to generate comprehensive ground truth positions that cater to both outdoor and indoor environments, thereby facilitating a robust evaluation of C-SLAM algorithms across diverse real-world scenarios.

### D. Trajectory Paradigms

The S3E dataset incorporates a diverse set of trajectory paradigms to simulate various collaborative scenarios that agents may encounter during SLAM operations. As depicted in Figure 4, we have designed these paradigms to address different loop closure conditions, both within individual agents (intra-loop) and across multiple agents (inter-loop). The following are the four trajectory paradigms we have included in our dataset:

**Concentric Circles:** In this paradigm, multiple unmanned platforms move in a coordinated formation, maintaining inter-connectivity and observing consistent environmental data. This setup enables continuous loop detection among platforms, enhancing the system’s ability to perform comprehensive area

Table III: Comparative Analysis of Trajectory Paradigms for Loop Closure Detection in C-SLAM. The symbols within the table indicate the presence (●) or absence (○) of loop closures for each paradigm, providing a quick reference for the suitability of each strategy in different collaborative robotic missions.

Trajectory Paradigm	Closures		Applications
	Intra-loop	Inter-loop	
Concentric Circles	●	●	Extensive coverage and detailed exploration
Intersecting Circles	●	●	Distributed search and rescue operations
Intersection Curve	○	●	Large-scale distributed exploration, patrol, and mapping
Rays	○	○	Independent exploration and mapping

coverage and exploration tasks such as environmental monitoring and map construction. The real-time sharing of perceptual information and pose estimation results among platforms bolsters the system’s positioning and mapping accuracy. However, the high similarity of observed data may complicate the detection and management of dynamic environmental changes.

**Intersecting Circles:** This paradigm is characterized by individual unmanned platforms operating in distinct zones, exchanging perceptual information upon intersection. Communication is established only at these points, with partial environmental information overlap. The exchange of historical data for loop closure detection at intersections, along with independent loop closure capabilities of each platform, expands the exploration range and improves mission efficiency. The division of search areas reduces communication and coordination demands within the system. However, limited interaction between platforms may hinder the achievement of globally consistent mapping and positioning.

**Intersection Curve:** Unmanned platforms initiate from diverse starting points, intersect at designated locations, and converge at a common endpoint. Communication and loop closure detection occur only upon meeting, with partial environmental information overlap. This paradigm is adept for large-area distributed exploration and mapping, facilitating regular information exchange and loop closure detection to minimize cumulative errors. The independent exploration by each platform enhances task efficiency and coverage. However, higher navigation and control capabilities are required for planning suitable intersection points and paths.

**Rays:** In this paradigm, platforms depart from various starting points, moving independently until converging at a shared endpoint. Communication is restricted to the final convergence, with minimal environmental information overlap. The platforms can exchange historical information for loop closure detection at convergence, but lack individual loop closure detection capabilities. This paradigm is suitable for large-scale independent exploration and mapping tasks, such as post-disaster searches and mine explorations. It emphasizes the autonomous execution of tasks by each platform, relying on its perceptual and computational resources. The final convergence allows for historical information exchange and local map optimization. However, the scarcity of information exchange poses challenges for globally consistent mapping and positioning, necessitating advanced autonomous navigation and decision-

Table IV: Analysis of S3E dataset.

Scenario		Time[s]	Trajectory				Ground Truth	Length[m]			Size[GB]	Sensors			
Env.	Region		a	b	c	d		Alpha	Bob	Carol		Camera	IMU	LiDAR	UWB
Outdoor	v1.0	Square_1	460		✓		RTK	546.0	496.5	529.2	17.8	✓	✓	✓	✗
		Square_2	255			✓	RTK	-	250.6	246.4	9.4	✓	✓	✓	✗
		Library_1	454	✓			RTK	507.6	517.2	498.9	16.3	✓	✓	✓	✗
		Campus_Road_1	878		✓		RTK	920.5	995.9	1072.3	29.4	✓	✓	✓	✗
		Playground_1	298	✓			RTK	407.7	425.6	445.5	8.7	✓	✓	✓	✗
		Playground_2	222			✓	RTK	265.6	315.7	456.4	6.3	✓	✓	✓	✗
		Dormitory_1	671			✓	RTK	727.0	719.3	721.9	23.5	✓	✓	✓	✗
	v2.0	Square_3	466			✓	GNSS/INS	487.4	569.6	563.8	8.5	✗	✓	✓	✓
		Library_2	491	✓			GNSS/INS	521.6	523.9	520.3	9.3	✗	✓	✓	✓
		Campus_Road_2	1594	✓			GNSS/INS	1938.6	1934.2	1950.1	30.9	✗	✓	✓	✓
		Campus_Road_3	907	✓			GNSS/INS	983.3	967.6	986.9	17.5	✗	✓	✓	✓
		Playground_3	111		✓		GNSS/INS	84.7	91.3	110.7	1.8	✗	✓	✓	✓
		Tunnel_1	425	✓			GNSS/INS	521.9	502.4	501.1	8.2	✗	✓	✓	✓
Indoor	v1.0	Teaching_Building_1	798		✓		RTK	617.2	734.4	643.4	27.3	✓	✓	✓	✗
		Laboratory_1	292		✓		Motion Capture	147.7	161.5	141.0	9.6	✓	✓	✓	✗
		Laboratory_2	391		✓		Motion Capture	215.3	199.1	160.3	12.7	✓	✓	✓	✗
		Laboratory_3	410		✓		Motion Capture	219.1	202.2	204.2	13.3	✓	✓	✓	✗
		Laboratory_4	380	✓			Motion Capture	173.7	177.2	180.0	12.7	✓	✓	✓	✗

making.

Each paradigm is meticulously crafted to offer a robust framework for assessing C-SLAM algorithms across a multitude of real-world collaborative robotic applications. Table III provides a comparative analysis of the loop closure detection situations corresponding to these paradigms, highlighting their respective advantages and potential application areas.

#### E. Dataset Analysis

To align with the collaborative mission scenarios and to reflect the nuances of the four trajectory paradigms, we have strategically chosen a variety of complex and representative scenes across different areas within Sun Yat-sen University's Guangzhou East Campus for our data collection endeavors. The mobile platforms, comprising three tele-operated robots, are under human control to ensure safety during operations.

For an exhaustive overview of the trajectory paradigms applied, the lengths of the trajectories, and the types of sensors utilized for each sequence, please refer to Table IV. The dataset encompasses a diverse range of environments, including squares, libraries, and six additional regions, comprising a total of 13 outdoor and 5 indoor sequences. The aggregated size of all 18 sequences is over 263.2 gigabytes, with a combined duration of more than 475.2 minutes and an extensive operating distance surpassing 28.1 kilometers. On average, the sequences last for 527.9 seconds each, which validates the dataset's adequacy for extensive, long-term assessments of C-SLAM technologies.

Furthermore, the dataset encompasses a variety of trajectories that adhere to the paradigms outlined in Section III-D. This diversity is instrumental for rigorous testing and comparative analysis of different C-SLAM methodologies under various interactive conditions, such as intra-robot and inter-robot loop closures.

To thoroughly assess the accuracy and robustness of C-SLAM algorithms in complex, real-world scenarios, our dataset encompasses a diverse range of environments, each presenting unique challenges:

**Dormitory:** Characterized by high pedestrian traffic and the presence of dynamic objects such as pedestrians and

bicycles, dormitory areas challenge the perception and tracking abilities of unmanned platforms. Their regular architectural layouts offer an ideal setting for evaluating the precision and consistency of C-SLAM algorithms across multiple platforms.

**Campus Road:** Serving as critical connectors, campus roads are marked by long distances and expansive views. They test the endurance and large-scale exploration capabilities of unmanned platforms. Extensive data collection along these roads, including long-distance and multi-cycle datasets, provides a robust foundation for assessing the stability, accuracy, and efficiency of C-SLAM algorithms over extended operations.

**Playground:** As open areas with fewer obstructions, sports fields challenge feature extraction, registration, and optimization processes. Data collected at various times of day, including day and night, evaluates the adaptability of C-SLAM algorithms to different lighting conditions. Additionally, data from rapid motion scenarios assesses the algorithms' performance under significant motion.

**Laboratory:** Indoor environments like laboratories, with their confined spaces, complex layouts, and rich semantic content, challenge navigation, obstacle avoidance, and semantic mapping. The presence of various instruments and furniture makes laboratories suitable for testing the advanced scene understanding and mapping capabilities of C-SLAM algorithms.

**Teaching Building and Tunnel:** These areas, with their severe perceptual aliasing, pose significant challenges due to poor lighting in tunnels and similar geometric structures in corridors, which can lead to errors in data association. They test the robustness of C-SLAM algorithms in maintaining accurate positioning and mapping.

Furthermore, our dataset includes other distinctive regions such as libraries and squares, which contribute additional environmental features and perceptual challenges to the dataset's diversity and comprehensiveness. Figure 5 displays the various trajectory paradigms captured in outdoor environments within the S3E dataset. Our dataset encompasses a diverse array of challenging environments that are likely to be faced by C-SLAM algorithms in real-world deployments. These include dynamic settings with moving objects, prolonged operational



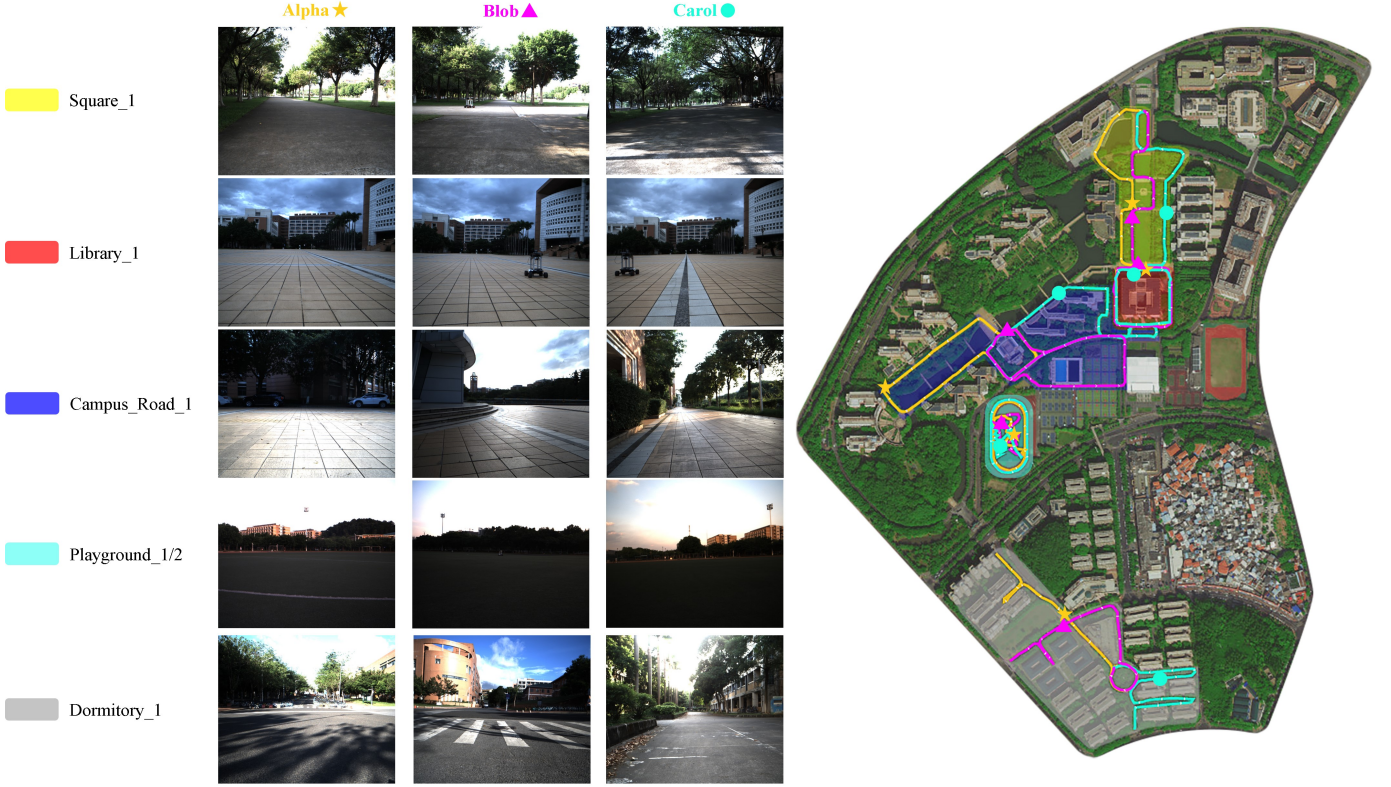


Figure 5: **Visualization of Outdoor Trajectory in the S3E Dataset.** The outdoor trajectories captured in the S3E dataset by three tele-operated mobile platforms, designated as Alpha, Bob, and Carol. The trajectories are distinctly annotated with Orange, Purple, and Cyan. The annotations  $\star$ ,  $\triangle$ , and  $\bullet$  indicate the specific positions where data was recorded in each sequence. The left portion of the figure presents the synchronized data capture at the annotated points, demonstrating the collaborative data collection process.

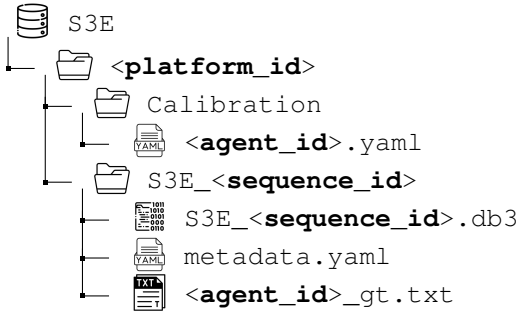


Figure 6: **S3E Dataset Organizational Structure.**

durations, scenarios with perceptual aliasing, indoor environments, and situations characterized by substantial motion. The inclusion of such a wide range of conditions lays a solid groundwork for an in-depth evaluation of the performance metrics, adaptability to different conditions, and overall robustness of C-SLAM algorithms. This thorough vetting process is essential for advancing the state-of-the-art in collaborative robotic navigation and mapping technologies.

#### F. Dataset Format

We employ the ROS2 [31] bag format for storing the sensor data, which is a widely-recognized standard in the robotics community. This format allows for efficient data management and playback, enabling users to simulate and analyze the dataset in various software environments. For the purpose

of simplifying data replay and ensuring seamless access to the synchronized sensor streams from our robotic platforms, we have implemented a consolidation strategy. Specifically, we merge the sensor data collected from the Alpha, Blob, and Carol robots during the same operational sequence into a single ROS2 bag file.

**Data Organization:** As depicted in Figure 6, our dataset features a well-organized directory structure. The calibration parameters are documented in YAML files and stored in the dedicated *Calibration* directory. Each sequence is accompanied by essential data files, including *.db3* file that house the primary sensor measurements, and *metadata.yaml* file that provide essential information about the sequence, such as sensor settings and capture conditions. Furthermore, to facilitate comprehensive performance evaluation, we have included auxiliary files such as *<agent\_id>\_gt.txt*, which contains the ground truth data.

**Ground Truth Format:** The ground truth data, which is essential for evaluating the accuracy of C-SLAM algorithms, is provided as TXT files. These files contain timestamped poses in UTM coordinates and orientation quaternions, formatted as follows:  $[timestamp, t_x, t_y, t_z, q_x, q_y, q_z, q_w]$ . The position  $t_{a \in \{x,y,z\}}$  denotes the robot's location in UTM coordinates, while  $q_{a \in \{x,y,z,w\}}$  represents the orientation in quaternion form.

**Sensor Data Topics:** Table V outlines the sensor topics included in the dataset, detailing the type of data each topic contains, its description, and the frequency of data capture.



Table V: Descriptions of ROS2 topics included in our dataset. Note that **agent\_id** stands for Alpha, Blob, and Carol.

Sensor	Topic	Type	Description	Frequency
LiDAR	<b>/agent_id/velodyne_points</b>	sensor_msgs/msg/PointCloud2	Raw velodyne pointcloud with $[x, y, z, intensity, ring, time]$	10 Hz
	<b>/agent_id/left_camera/compressed</b>	sensor_msgs/msg/CompressedImage	Compressed RGB8 image with $1224 \times 1024$	
Camera <sup>1</sup>	<b>/agent_id/right_camera/compressed</b>	sensor_msgs/msg/CompressedImage	Compressed RGB8 image with $1224 \times 1024$	10 Hz
IMU	<b>/agent_id/imu/data</b>	sensor_msgs/msg/Imu	Raw imu data	100 Hz
RTK <sup>2</sup>	<b>/agent_id/fix</b>	sensor_msgs/msg/NavSatFix	RTK-GNSS data with $[latitude, longitude, altitude]$	1 Hz
UWB <sup>3</sup>	<b>/agent_id/nlink_linktrack_nodeframe2</b>	std_msgs/msg/Float64MultiArray	UWB data comprises 13 data fields <sup>4</sup>	50 Hz
	<b>/agent_id/time_reference</b>	sensor_msgs/msg/TimeReference	GPS time reference anchored at the epoch of 1980-01-06 00:00:00 UTC	
	<b>/agent_id/fix</b>	sensor_msgs/msg/NavSatFix	RTK-GNSS data with $[latitude, longitude, altitude]$	
GNSS/INS <sup>3</sup>	<b>/agent_id/correct_imu</b>	sensor_msgs/msg/Imu	Raw build-in imu data	100 Hz
	<b>/agent_id/vel</b>	geometry_msgs/msg/TwistStamped	Timestamped linear velocities ( $m/s$ ) of mobile platform along $[east, north, up]$	
	<b>/agent_id/heading</b>	geometry_msgs/msg/QuaternionStamped	Timestamped quaternions map mobile platform attitudes	

<sup>1</sup> Available in all sequences of S3Ev1.0. <sup>2</sup> Available in outdoor sequences of S3Ev1.0. <sup>3</sup> Available in all sequences of S3Ev2.0.

<sup>4</sup> Detailed definitions of UWB data fields are documented and accessible on our project website.

Table VI: ATE [ $m$ ] for Single SLAM and C-SLAM in the S3Ev1.0 outdoor environment without UWB measurement.  $\alpha$ ,  $\beta$ , and  $\gamma$  stand for Alpha, Bob, and Carol respectively.  $\times$  fails to initialize or track frames. If inter-loop closures detection fails, we mark it “Failed”.

Methods	Square_1			Square_2			Library_1			Campus_Road_1			Playground_1			Playground_2			Dormitory_1		
	$\alpha$	$\beta$	$\gamma$	$\alpha$	$\beta$	$\gamma$	$\alpha$	$\beta$	$\gamma$	$\alpha$	$\beta$	$\gamma$	$\alpha$	$\beta$	$\gamma$	$\alpha$	$\beta$	$\gamma$	$\alpha$	$\beta$	$\gamma$
ORB-SLAM3	1.16	15.5	$\times$	-	2.81	$\times$	11.4	$\times$	$\times$	$\times$	55.5	$\times$	0.87	$\times$	$\times$	3.29	$\times$	$\times$	-	$\times$	
VINS-Fusion	1.81	$\times$	4.83	-	1.51	0.62	7.95	7.86	5.56	$\times$	16.5	$\times$	3.24	7.36	4.31	31.3	$\times$	$\times$	6.67	3.97	7.70
LIO-SAM	1.19	1.75	$\times$	-	0.73	0.36	1.12	1.52	1.14	2.06	3.25	2.43	$\times$	$\times$	0.86	$\times$	$\times$	0.68	0.63	1.44	0.91
LVI-SAM	1.21	0.88	$\times$	-	0.79	0.40	1.89	1.67	1.31	2.44	3.14	1.30	$\times$	1.59	0.76	6.78	6.10	0.72	0.86	1.48	0.94
CoLRIO (front-end)	<b>0.90</b>	0.57	0.65	-	<b>0.49</b>	<b>0.19</b>	1.37	1.54	<b>0.88</b>	<b>1.06</b>	0.91	1.10	0.39	0.45	0.20	0.69	0.35	0.29	<b>0.47</b>	<b>0.83</b>	0.81
COVINS	1.63	0.83	1.75	Failed			$\times$			18.3	9.61	54.7	$\times$			$\times$			$\times$		
DiSCo-SLAM	Failed			Failed			0.74	1.33	1.27	2.21	1.35	Failed	<b>0.27</b>	<b>0.37</b>	0.38	$\times$			0.54	1.47	Failed
Swarm-SLAM	8.13	7.11	2.13	-	1.39	0.52	3.16	2.71	3.22	7.62	11.3	6.36	3.36	3.38	1.70	1.36	1.32	2.05	10.0	5.61	4.50
DCL-SLAM	1.23	0.86	<b>0.66</b>	-	0.50	0.26	<b>0.58</b>	1.26	1.17	1.51	1.48	1.87	0.33	0.40	0.32	$\times$			0.52	1.37	<b>0.51</b>
CoLRIO	0.91	<b>0.53</b>	0.80	-	0.56	0.20	1.06	<b>1.05</b>	1.02	1.08	<b>0.79</b>	<b>1.08</b>	0.39	0.60	<b>0.16</b>	<b>0.44</b>	<b>0.32</b>	<b>0.29</b>	0.54	0.87	0.84

Table VII: ATE [ $m$ ] for Single SLAM and C-SLAM in the S3Ev1.0 indoor environment without UWB measurement.  $\alpha$ ,  $\beta$ , and  $\gamma$  stand for Alpha, Bob, and Carol respectively.

Methods	Laboratory_1			Laboratory_2			Laboratory_3			Laboratory_4		
	$\alpha$	$\beta$	$\gamma$	$\alpha$	$\beta$	$\gamma$	$\alpha$	$\beta$	$\gamma$	$\alpha$	$\beta$	$\gamma$
LIO-SAM	0.47	1.82	2.51	12.2	6.12	8.88	6.24	8.57	7.31	1.96	0.88	0.65
FAST-LIO2	7.27	11.2	5.13	10.2	2.14	15.0	12.8	6.80	7.33	0.79	0.88	0.37
CoLRIO (front-end)	<b>0.40</b>	0.51	0.44	0.83	0.79	0.96	1.79	0.91	2.43	<b>0.67</b>	0.65	0.87
DiSCo-SLAM	0.56	<b>0.43</b>	<b>0.33</b>	2.02	0.36	4.60	2.01	<b>0.31</b>	1.28	1.40	2.02	3.45
Swarm-SLAM	9.86	1.14	3.29	4.56	7.03	15.3	7.06	12.2	8.10	1.79	3.40	3.47
CoLRIO	0.43	0.50	0.44	<b>0.40</b>	<b>0.07</b>	<b>0.08</b>	<b>0.49</b>	0.91	<b>0.13</b>	0.95	<b>0.65</b>	<b>0.18</b>

#### IV. EXPERIMENTS

##### A. Baselines

We have implemented four single-agent SLAM systems, namely ORB-SLAM3 [32], VINS-Fusion [33], LIO-SAM [34], and LVI-SAM [35]. Additionally, we have incorporated five collaborative SLAM (C-SLAM) systems into our study, which include COVINS [2], DiSCo-SLAM [3], Swarm-SLAM [24], DCL-SLAM [4], and CoLRIO [5]. These systems have been evaluated using the S3E dataset.

For most of the baselines, we only modify the intrinsic and extrinsic of the sensors and use the left camera for evaluation.



Figure 7: Map in Laboratory\_1 with CoLRIO.

Table VIII: ATE [m] for C-SLAM in the S3Ev2.0 outdoor environment with UWB measurement.  $\alpha$ ,  $\beta$ , and  $\gamma$  stand for Alpha, Bob, and Carol respectively.

Methods	Square_3			Library_2			Campus_Road_2			Campus_Road_3			Playground_3			Tunnel_1		
	$\alpha$	$\beta$	$\gamma$	$\alpha$	$\beta$	$\gamma$	$\alpha$	$\beta$	$\gamma$	$\alpha$	$\beta$	$\gamma$	$\alpha$	$\beta$	$\gamma$	$\alpha$	$\beta$	$\gamma$
DiSCo-SLAM	<b>1.15</b>	<b>1.26</b>	12.11	1.07	1.02	0.98	15.41	14.60	3.37	1.27	1.32	39.76	9.01	0.72	2.32	5.06	11.90	4.40
Swarm-SLAM	8.52	5.64	2.80	3.15	0.91	0.94	48.96	64.23	22.37	8.79	9.60	4.90	1.11	3.24	5.47	10.49	11.06	10.06
CoLRIO (w/o UWB)	1.79	1.62	<b>1.30</b>	0.91	0.89	0.88	<b>1.29</b>	2.97	<b>1.21</b>	1.04	1.13	1.07	0.24	<b>0.19</b>	0.30	5.49	4.69	5.15
CoLRIO (w UWB)	1.71	1.52	1.54	<b>0.89</b>	<b>0.87</b>	<b>0.88</b>	1.37	<b>1.59</b>	1.34	<b>0.77</b>	<b>0.61</b>	<b>0.90</b>	<b>0.23</b>	0.20	<b>0.30</b>	<b>4.01</b>	<b>3.21</b>	<b>3.60</b>

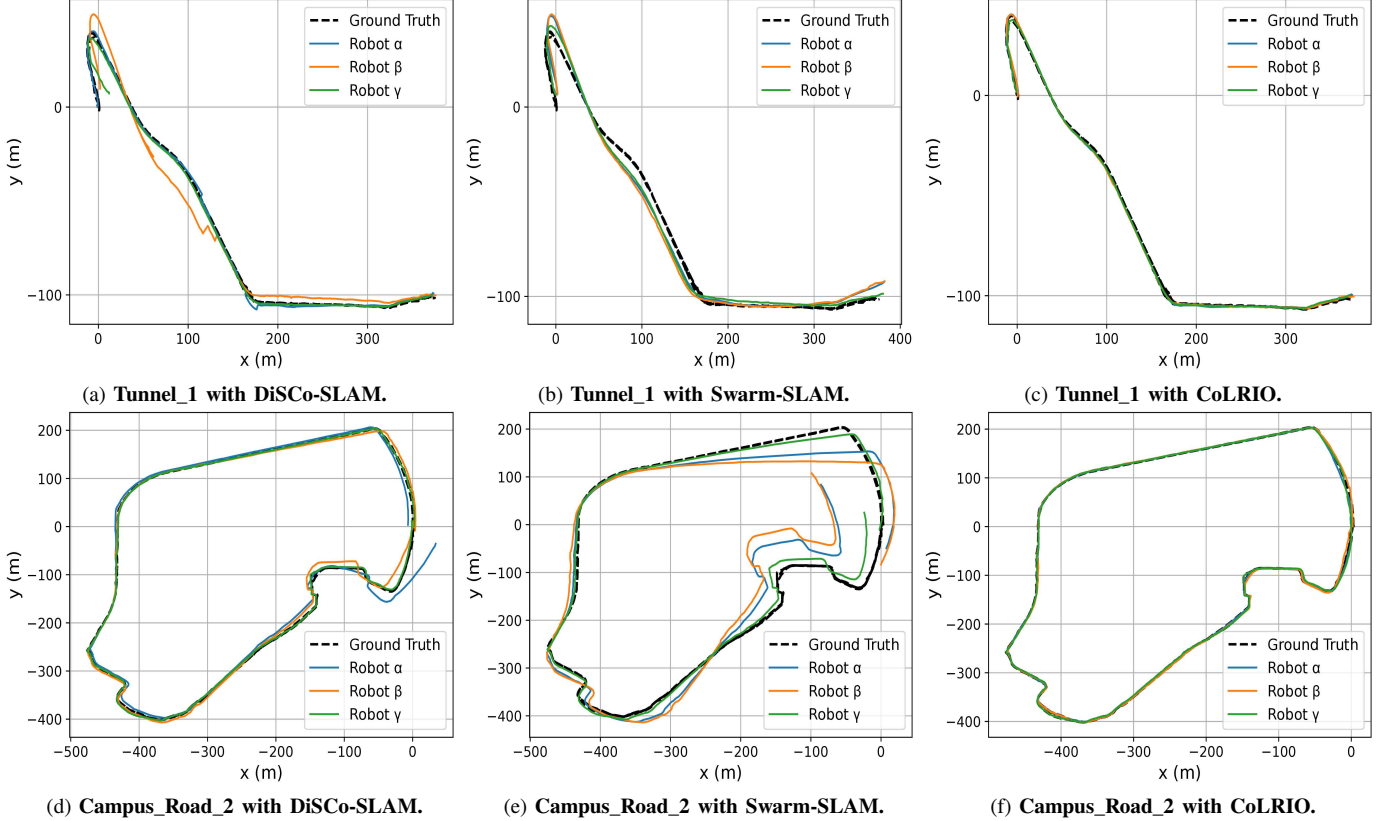


Figure 8: The qualitative results of outdoor environments.

environments without UWB measurement.

#### • Key Findings:

- **Inter-Loop Closures Detection Impact:** The results highlight the increased performance of C-SLAM systems when successful in detecting inter-loop closures, showcasing the benefits of collaborative information sharing among agents.
- **Front-end State Estimation Impact:** The performance of C-SLAM is heavily influenced by the accuracy of its front-end state estimation. For example, CoLRIO's success in certain scenarios is attributed to its effective front-end tracker.

#### • Specific Observations:

- In scenarios with large spatial overlap, C-SLAM systems leveraged inter-robot measurements to enhance state estimation accuracy. However, in areas with limited overlap, reducing drift remained a challenge.
- The incorporation of UWB measurements in CoLRIO significantly improved localization robustness

(a) Teaching\_building\_1.

(b) Square\_1.

Figure 9: *The animations of S3E dataset.* For an optimal viewing experience, we recommend using *Adobe Reader / KDE Okular*, as these applications provide the necessary support for smooth playback and clear visualization of the animated sequences.

## B. Results

Our experimental evaluation of the S3E dataset provides valuable insights into the performance of various state-of-the-art SLAM methodologies under diverse real-world conditions. The results, summarized in Table VI and Table VII, reveal the absolute trajectory error (ATE) for both single-agent and collaborative SLAM (C-SLAM) systems in outdoor and indoor

and accuracy, as demonstrated in Table VIII, showcasing the benefits of additional ranging data for C-SLAM systems.

The results from our experiments on the S3E dataset underscore the importance of continuous innovation in C-SLAM algorithms. The varying performance across different scenarios and the impact of collaborative data sharing highlight the need for further research. The qualitative results presented in Figure 7 and Figure 8, along with the animations in Figure 9, visually complement the performance metrics, providing a deeper understanding of the C-SLAM systems' behavior in diverse environments.

## V. CONCLUSION

In conclusion, the S3E dataset represents a significant advancement in the field of Collaborative Simultaneous Localization and Mapping (C-SLAM). Its expansive and multimodal nature, coupled with the introduction of four distinct trajectory paradigms, provides an unparalleled platform for evaluating C-SLAM systems across a multitude of real-world scenarios. Captured across various indoor and outdoor environments, the dataset includes meticulously synchronized streams from a range of sensors, offering an unprecedented level of detail and complexity. Our experiments utilizing this dataset have highlighted the improved robustness of C-SLAM systems, especially in their ability to handle inter-loop closures. The incorporation of UWB measurements has further enhanced the accuracy and reliability of localization within these systems. The S3E dataset serves not only as a benchmark for current C-SLAM methodologies but also as a catalyst for future innovations in multi-agent robotic navigation and mapping. We anticipate that this dataset will inspire further research and development, pushing the boundaries of what is possible in collaborative robotic systems.

## REFERENCES

- [1] B. D. Gouveia, D. Portugal, D. C. Silva, and L. Marques, "Computation sharing in distributed robotic systems: a case study on slam," *IEEE Transactions on Automation Science and Engineering*, vol. 12, no. 2, pp. 410–422, 2014.
- [2] P. Schmuck, T. Ziegler, M. Karrer, J. Perraudin, and M. Chli, "Covins: Visual-inertial slam for centralized collaboration," in *2021 IEEE International Symposium on Mixed and Augmented Reality Adjunct (ISMAR-Adjunct)*, Oct 2021, pp. 171–176.
- [3] Y. Huang, T. Shan, F. Chen, and B. Englot, "Disco-slam: Distributed scan context-enabled multi-robot lidar slam with two-stage global-local graph optimization," *IEEE Robotics and Automation Letters*, vol. 7, no. 2, pp. 1150–1157, April 2022.
- [4] S. Zhong, Y. Qi, Z. Chen, J. Wu, H. Chen, and M. Liu, "Dcl-slam: A distributed collaborative lidar slam framework for a robotic swarm," *IEEE Sensors Journal*, 2023.
- [5] S. Zhong, H. Chen, Y. Qi, D. Feng, Z. Chen, J. Wu, W. Wen, and M. Liu, "Colrio: Lidar-ranging-inertial centralized state estimation for robotic swarms," *arXiv preprint arXiv:2402.11790*, 2024.
- [6] X. Liu, S. Wen, J. Zhao, T. Z. Qiu, and H. Zhang, "Edge-assisted multi-robot visual-inertial slam with efficient communication," *IEEE Transactions on Automation Science and Engineering*, 2024.
- [7] M. Mishra, P. Poddar, R. Agrawal, J. Chen, P. Tokekar, and P. Sujit, "Multi-agent deep reinforcement learning for persistent monitoring with sensing, communication, and localization constraints," *IEEE Transactions on Automation Science and Engineering*, 2024.
- [8] P.-Y. Lajoie, B. Ramtoula, F. Wu, and G. Beltrame, "Towards collaborative simultaneous localization and mapping: a survey of the current research landscape," *Field Robotics*, vol. 2, no. 1, pp. 971–1000, mar 2022.
- [9] A. Geiger, P. Lenz, C. Stiller, and R. Urtasun, "Vision meets robotics: The kitti dataset," *The International Journal of Robotics Research*, vol. 32, no. 11, pp. 1231–1237, 2013.
- [10] M. Burri, J. Nikolic, P. Gohl, T. Schneider, J. Rehder, S. Omari, M. W. Achtelik, and R. Siegwart, "The euroc micro aerial vehicle datasets," *The International Journal of Robotics Research*, vol. 35, no. 10, pp. 1157–1163, 2016.
- [11] K. Y. Leung, Y. Halpern, T. D. Barfoot, and H. H. Liu, "The utias multi-robot cooperative localization and mapping dataset," *The International Journal of Robotics Research*, vol. 30, no. 8, pp. 969–974, 2011.
- [12] S. Agarwal, A. Vora, G. Pandey, W. Williams, H. Kourous, and J. McBride, "Ford multi-av seasonal dataset," *The International Journal of Robotics Research*, vol. 39, no. 12, pp. 1367–1376, 2020.
- [13] R. Dubois, A. Eudes, and V. Frémont, "Airmuseum: a heterogeneous multi-robot dataset for stereo-visual and inertial simultaneous localization and mapping," in *2020 IEEE International Conference on Multi-sensor Fusion and Integration for Intelligent Systems (MFI)*, Sep. 2020, pp. 166–172.
- [14] Y. Tian, Y. Chang, L. Quang, A. Schang, C. Nieto-Granda, J. P. How, and L. Carlone, "Resilient and distributed multi-robot visual slam: Datasets, experiments, and lessons learned," in *2023 IEEE/RSJ International Conference on Intelligent Robots and Systems (IROS)*. IEEE, 2023, pp. 11 027–11 034.
- [15] Y. Zhu, Y. Kong, Y. Jie, S. Xu, and H. Cheng, "Graco: A multimodal dataset for ground and aerial cooperative localization and mapping," *IEEE Robotics and Automation Letters*, vol. 8, no. 2, pp. 966–973, 2023.
- [16] S. Zhao, Y. Gao, T. Wu, D. Singh, R. Jiang, H. Sun, M. Sarawata, Y. Qiu, W. Whittaker, I. Higgins *et al.*, "Subt-mrs dataset: Pushing slam towards all-weather environments," in *Proceedings of the IEEE/CVF Conference on Computer Vision and Pattern Recognition*, 2024, pp. 22 647–22 657.
- [17] B. Cao, C.-N. Ritter, K. Alomari, and D. Goehring, "Cooperative lidar localization and mapping for v2x connected autonomous vehicles," in *2023 IEEE/RSJ International Conference on Intelligent Robots and Systems (IROS)*. IEEE, 2023, pp. 11 019–11 026.
- [18] R. Pyla, V. Pandalaneni, P. J. N. Raju *et al.*, "Design and development of swarm agv's alliance for search and rescue operations," *Journal of Robotics and Control (JRC)*, vol. 4, no. 6, pp. 791–807, 2023.
- [19] R. Dubé, A. Cramariuc, D. Dugas, H. Sommer, M. Dymczyk, J. Nieto, R. Siegwart, and C. Cadena, "Segmap: Segment-based mapping and localization using data-driven descriptors," *The International Journal of Robotics Research*, vol. 39, no. 2-3, pp. 339–355, 2020.
- [20] K. Ebadi, Y. Chang, M. Palieri, A. Stephens, A. Hatteland, E. Heiden, A. Thakur, N. Funabiki, B. Morrell, S. Wood, L. Carlone, and A.-a. Agha-mohammadi, "Lamp: Large-scale autonomous mapping and positioning for exploration of perceptually-degraded subterranean environments," in *2020 IEEE International Conference on Robotics and Automation (ICRA)*, May 2020, pp. 80–86.
- [21] T. Cieslewski, S. Choudhary, and D. Scaramuzza, "Data-efficient decentralized visual slam," in *2018 IEEE International Conference on Robotics and Automation (ICRA)*, May 2018, pp. 2466–2473.
- [22] S. Choudhary, L. Carlone, C. Nieto, J. Rogers, H. I. Christensen, and F. Dellaert, "Distributed mapping with privacy and communication constraints: Lightweight algorithms and object-based models," *The International Journal of Robotics Research*, vol. 36, no. 12, pp. 1286–1311, 2017.
- [23] P.-Y. Lajoie, B. Ramtoula, Y. Chang, L. Carlone, and G. Beltrame, "Door-slam: Distributed, online, and outlier resilient slam for robotic teams," *IEEE Robotics and Automation Letters*, vol. 5, no. 2, pp. 1656–1663, April 2020.
- [24] P.-Y. Lajoie and G. Beltrame, "Swarm-slam: Sparse decentralized collaborative simultaneous localization and mapping framework for multi-robot systems," *IEEE Robotics and Automation Letters*, vol. 9, no. 1, pp. 475–482, 2023.
- [25] C. Forster, S. Lynen, L. Kneip, and D. Scaramuzza, "Collaborative monocular slam with multiple micro aerial vehicles," in *2013 IEEE/RSJ International Conference on Intelligent Robots and Systems*, Nov 2013, pp. 3962–3970.
- [26] J. L. Schönberger and J.-M. Frahm, "Structure-from-motion revisited," in *2016 IEEE Conference on Computer Vision and Pattern Recognition (CVPR)*, June 2016, pp. 4104–4113.
- [27] Z. Zhang, "A flexible new technique for camera calibration," *IEEE Transactions on Pattern Analysis and Machine Intelligence*, vol. 22, no. 11, pp. 1330–1334, Nov 2000.



- [28] N. El-Sheimy, H. Hou, and X. Niu, "Analysis and modeling of inertial sensors using allan variance," *IEEE Transactions on instrumentation and measurement*, vol. 57, no. 1, pp. 140–149, 2007.
- [29] P. Furgale, J. Rehder, and R. Siegwart, "Unified temporal and spatial calibration for multi-sensor systems," in *2013 IEEE/RSJ International Conference on Intelligent Robots and Systems*, Nov 2013, pp. 1280–1286.
- [30] L. Zhou, Z. Li, and M. Kaess, "Automatic extrinsic calibration of a camera and a 3d lidar using line and plane correspondences," in *2018 IEEE/RSJ International Conference on Intelligent Robots and Systems (IROS)*, Oct 2018, pp. 5562–5569.
- [31] S. Macenski, T. Foote, B. Gerkey, C. Lalancette, and W. Woodall, "Robot operating system 2: Design, architecture, and uses in the wild," *Science robotics*, vol. 7, no. 66, p. eabm6074, 2022.
- [32] C. Campos, R. Elvira, J. J. G. Rodríguez, J. M. M. Montiel, and J. D. Tardós, "Orb-slam3: An accurate open-source library for visual, visual-inertial, and multimap slam," *IEEE Transactions on Robotics*, vol. 37, no. 6, pp. 1874–1890, Dec 2021.
- [33] T. Qin, J. Pan, S. Cao, and S. Shen, "A general optimization-based framework for local odometry estimation with multiple sensors," *arXiv preprint arXiv:1901.03638*, 2019.
- [34] T. Shan, B. Englot, D. Meyers, W. Wang, C. Ratti, and D. Rus, "Lio-sam: Tightly-coupled lidar inertial odometry via smoothing and mapping," in *2020 IEEE/RSJ International Conference on Intelligent Robots and Systems (IROS)*, Oct 2020, pp. 5135–5142.
- [35] T. Shan, B. Englot, C. Ratti, and D. Rus, "Lvi-sam: Tightly-coupled lidar-visual-inertial odometry via smoothing and mapping," in *2021 IEEE International Conference on Robotics and Automation (ICRA)*, May 2021, pp. 5692–5698.



**Dapeng Feng** received the B.E. degree in Computer Science and Technology from Guangdong University of Foreign Studies, Guangzhou, China, in 2018 and the M.S. degree in Pattern Recognition and Intelligent Systems with Sun Yat-sen University, Guangzhou, China, in 2021.

He is currently pursuing the Ph.D. degree in Computer Science and Technology with Sun Yat-sen University, Guangzhou, China. He has published several cutting-edge projects on computer vision and robotics, including 3d object detection and SLAM.



**Yuhua Qi** received the Ph. D. degree in Aerospace Engineering from Beijing Institute of Technology, Beijing, China, in 2020.

He is currently an Associate Researcher with Sun Yat-sen University, Guangzhou, China. His research endeavors are centered on several key areas within the realm of robotics and autonomous systems. Specifically, his work encompasses cooperative control strategies, aimed at enhancing the collective performance of robot teams, and the broader domain of autonomous unmanned systems.



**Shipeng Zhong** received the Ph.D. degree in Computer Science and Technology with Sun Yat-sen University, Guangzhou, China, in 2024.

He is currently a Researcher with WeRide, Guangzhou, China. His research is focused on the cutting-edge domains of autonomous unmanned systems and cooperative mapping. His work is aimed at advancing the capabilities of these systems to operate with greater autonomy and to collaborate effectively in complex environments.



**Zhiqiang Chen** received the B.E. degree in Information Engineering from Sun Yat-sen University, Guangzhou, China, in 2021 and the M.S. degree in Computer Science and Technology with Sun Yat-sen University, Guangzhou, China, in 2024.

He is currently pursuing the Ph.D. degree with The University of Hong Kong, Hong Kong SAR, China. His research interests are concentrated in the innovative applications of SLAM. His work is also deeply engaged with the intricate processes of integrating data from multiple sources to enhance

the accuracy and reliability of robotic systems.



**Qiming Chen** received the B.E. degree in Wood Science and Engineering from South China Agricultural University, Guangzhou, China, in 2022.

He is currently a Research Assistant with Sun Yat-sen University, Guangzhou, China. His research interests are primarily in the area of mechanical design.



**Hongbo Chen** received the Ph.D. degree in Aircraft Design and Engineering from Harbin Institute of Technology, Harbin, China, in 2007.

He is currently a Professor with Sun Yat-sen University, Guangzhou, China. His research and system engineering endeavors are primarily concentrated in the cutting-edge areas of Causal Artificial Intelligence (AI) theory and application, as well as aerospace intelligent unmanned systems.



**Jin Wu** (Member, IEEE) received the B.S. degree from University of Electronic Science and Technology of China, Chengdu, China. He is currently pursuing the Ph.D. degree with The Hong Kong University of Science and Technology, Hong Kong SAR, China.

Till now, his related research works have been reported in over 140 journal and conference papers, which include top-tier publications, such as T-RO, T-CAS, T-MECH, T-ASE, T-CYB, and T-AES. His research falls within the algorithmic foundations

for robotics with particular focuses on attitude/pose estimation and related mechatronic systems design/control, numerical optimization, deep learning, and high-performance computing.



**Jun Ma** received the Ph.D. degree in Electrical and Computer Engineering from National University of Singapore, Singapore, in 2018.

He is currently an Assistant Professor with the Robotics and Autonomous Systems Thrust, The Hong Kong University of Science and Technology (Guangzhou), Guangzhou, China; an Assistant Professor with the Division of Emerging Interdisciplinary Areas and an Affiliate Assistant Professor with the Department of Electronic and Computer Engineering, The Hong Kong University of Science

and Technology, Hong Kong SAR, China. His research interests include control, optimization, and machine learning with application to robotics and autonomous driving.